Quantum battery with ultracold atoms: Bosons versus fermions

Tanoy Kanti Konar, Leela Ganesh Chandra Lakkaraju, Srijon Ghosh, and Aditi Sen(De)
Harish-Chandra Research Institute, A CI of Homi Bhabha National Institute, Chhatnag Road, Jhunsi, Prayagraj 211 019, India

(Received 3 July 2022; accepted 28 July 2022; published 29 August 2022)

We design a quantum battery made up of bosons or fermions in an ultracold-atom setup, described by *Fermi-Hubbard* and *Bose-Hubbard* models, respectively. We compare the performance of bosons and fermions to determine which can function as a quantum battery more effectively given a particular on-site interaction and initial state temperature. The performance of a quantum battery is quantified by the maximum energy stored per unit time over the evolution under an on-site charging Hamiltonian. We report that when the initial battery state is in the ground state, fermions outperform bosons in a certain configuration over a large range of on-site interactions which are shown analytically for a smaller number of lattice sites and numerically for a considerable number of sites. Bosons take the lead when the temperature is comparatively high in the initial state for a longer range of on-site interaction. We study a number of up and down fermions as well as the number of bosons per site to find the optimal filling factor for maximizing the average power of the battery. We also introduce disorder in both on-site and hopping parameters and demonstrate that the maximum average power is robust against impurities. Moreover, we identify a range of tuning parameters in the fermionic and bosonic systems where the disorder-enhanced power is observed.

DOI: 10.1103/PhysRevA.106.022618

I. INTRODUCTION

In recent years, tremendous efforts have been devoted to developing the avenue of quantum technologies, which includes the advancement of miniaturized quantum devices [1], that are indispensable for various practical purposes. Such quantum gadgets have been shown to outperform the existing classical ones in different sectors ranging from metrology [2], cryptography [3], and cybersecurity to data analysis and computing [4]. The development of smaller, and more effective devices naturally leads to the realm of quantum mechanics. In this respect, microscopic thermodynamic devices have also been shown to provide remarkable precision in thermometry [5], thereby contributing to the field of quantum thermodynamics [6,7]. To explore and model quantum thermal machines such as quantum refrigerators [1,8–12] and quantum batteries [13–23], modified definitions of work, heat, and entropy are introduced that can take into account the effects of quantumness in the system.

The behavior of traditional chemical batteries that can store energy is purely classical in nature and hence cannot be used in quantum-mechanical apparatuses. With this requirement, Alicki and Fannes first proposed the concept of a quantum battery (QB) [13], a d-dimensional quantum-mechanical system composed of N noninteracting subsystems which are able to store energy for future use and can efficiently be charged by global entangling operations. After the initial proposal, several interesting works were reported [23], which include quantum batteries with the Dicke state [24,25], the role of entanglement production in the process of work extraction [16,26], nonlocal charging with an extensive advantage in power storage [27], and the effects of decoherence on quantum batteries [22,28–32]. Specifically, it was reported that when the battery is in contact with the environment, in the presence of both Markovian and non-Markovian noises, non-Markovian noise can sometimes help to extract a high amount of work depending upon the system parameters [22,30]. On the other hand, interacting spin systems composed of spin-s particles can also be used to design QBs which can be charged via a local magnetic field [18,33,34]. In a similar spirit, the nearest-neighbor hopping interaction of a spin chain acts as a battery and, coupled with a cavity mode, has been shown to enhance the capability of storing energy in the system [15]. More importantly, quantum batteries have been realized on different platforms like solid-state systems, where either each of the two-level systems is enclosed in a single cavity or the ensembles of two-level systems are in a single cavity [24,35], and superconducting circuits, which can be charged by using an external magnetic field [36].

In this work, we propose to design a quantum battery with a one-dimensional *Hubbard model*, which is realizable via cold atoms in an optical lattice, where the lattice is filled up with either fermions or bosons and is well described by the *Fermi-Hubbard* (FH) and *Bose-Hubbard* (BH) [37–40] models, respectively (see Fig. 1). Specifically, the initial state of the battery is prepared as the ground or canonical equilibrium states of the FH and BH models, while the charging of the battery can take place by tuning the strength of the on-site intra-atomic interactions. It is important to stress here that in all the aforementioned proposals of QBs, the subsystems are distinguishable because their positions are fixed in space, while in the current proposal, the particles can hop from one lattice site to another and, as a consequence, become indistinguishable within the lattice system. We also know

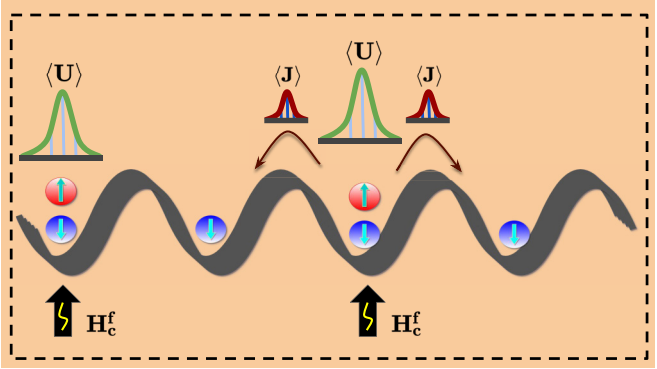

FIG. 1. Schematic representation of a quantum battery based on a one-dimensional Fermi-Hubbard Hamiltonian with and without disorder with L lattice sites. H_c^f in Eq. (3) is used to charge the battery. As shown in the text, similar modeling of QB is also possible with the Bose-Hubbard system. Notice that the charging part solely depends on the on-site interaction term U_i^μ $(\mu = b, f)$, which is nonvanishing for a particular lattice site only when at least two particles are present at each lattice. However, there are hopping terms for any two sites which we have not shown for all sites to make the schematics less cumbersome. We also report the robustness observed in the performance of the QB against different kinds of disorder present in the on-site and hopping strengths.

that both models possess rich phase diagrams with phases like Mott-insulator, superfluid, superconducting, Fermi-liquid [37,41,42], and density-wave, Haldane-insulator phases in the extended BH model [43,44], and hence such a study may connect physical properties of the bosonic and fermionic systems with quantum thermodynamics.

A comparative study carried out between the FH and the BH models reveals that fermionic batteries with more than two lattice sites can store a higher amount of extractable power output than those of bosonic systems, provided the repulsive or attractive on-site interactions are suitably tuned by varying the scattering lengths and the initial state of the battery is at the zero temperature with half filling. The hierarchy is reversed, i.e., the batteries made up of BH models demonstrate an advantage over the FH ones, when the initial state is prepared at a finite and high temperature. We also illustrate that apart from the ratio between the intra-atomic on-site and interatomic hopping interactions, the patterns of the power output also depend on the even and odd lattice sites in both models. For a fixed lattice site, we optimize the maximum average power output over configurations allowed for fermions and bosons, where in the latter case, we also fix the particles per site and observe that the optimized power decreases (increases) with the increase of lattice sites (the increase of the particles per site) for fermions (bosons).

With the significant advancement in experiments having different physical substrates, the disordered quantum systems [45–49] are of great interest to study since it is almost impossible to prepare a system while avoiding impurities in laboratories. In particular, although a high level of control to generate and manipulate ultracold bosonic or fermionic gases or their mixtures has been achieved experimentally, there is always a possibility of including disorder during the transfer of the samples to optical lattices. Disorder in the hopping parameter of the Hubbard Hamiltonian can also be realized by modulating the applied electric field of the laser or by doping impurities in the system. Impurities can also appear by aid of additional lattices or by modulating magnetic fields in the system [37,50]. Interestingly, cold atomic systems turn out to be one of the experimentally friendly platforms where disordered systems can be realized and engineered.

Although, intuitively, disorder detrimentally affects the characteristics of quantum systems and hence their performance, this was shown to be not true [18,34,51–58]; that is, certain features of the quantum system are found to get enhanced even in the presence of impurities. Moreover, disordered systems show a lot of counterintuitive phenomena, which include Anderson localization [59], many-body localization which pinpoints the distinction between thermalization and the localized phase [60–63], and high-temperature superconductivity [64], to name a few. In this respect, we show that the quenched averaged power outputs are robust against random hopping and random on-site interactions in both FH and BH models. In the case of disorder introduced in hopping, we report that there is a regime of the hopping strength in which both bosonic and fermionic disordered systems can produce higher maximal power than that of the ordered ones, which we refer to as the *disorder-enhanced power*. Such an increment in power can be seen due to the monotonically increasing nature of power in batteries with an ordered Hamiltonian. The randomness in hopping and on-site interactions are chosen from Gaussian and uniform distributions with a fixed mean and standard deviations, and both types of randomness can be realized in the cold atomic setup.

This paper is organized in the following manner. The design of quantum batteries based on Hubbard models and their charging processes are introduced in Sec. II. In Sec. III, the performance of the QB is studied, and comparative studies between bosonic and fermionic systems are carried out. In Sec. IV, the effects of the filling factor and the temperature of the initial state are investigated, while the disordered BH and FH models are considered as batteries in Sec. V. Finally, concluding remarks are given in Sec. VI.

II. MODELING A QUANTUM BATTERY USING HUBBARD HAMILTONIANS

We model a quantum battery as a one-dimensional Hubbard Hamiltonian (see Fig. 1 for a schematic representation) with L lattice sites filled with fermions or bosons, known as the Fermi-Hubbard and Bose-Hubbard models, respectively, which can be engineered in the laboratory with cold atoms in optical lattices [37,38]. Such a study also identifies the regime where fermionic systems show better performance as a QB than that of the bosonic ones and vice versa.

Model of the battery. The initial state of a quantum battery [13,18,33] is taken as the ground state or the canonical equilibrium state, i.e., $\rho_{th} = \frac{e^{-\beta' H_B^\mu}}{Z}$ $(\mu = f, b)$, of the Fermi-Hubbard or Bose-Hubbard Hamiltonian H_B^μ, where the superscript represents fermionic or bosonic systems. Here $\beta' = \frac{1}{k_B T}$, with k_B being the Boltzmann constant, T being the absolute temperature, and the partition function $Z = \mathrm{Tr}(e^{-\beta' H_B^\mu})$. When the lattice sites are occupied with fermions,

the *Fermi-Hubbard Hamiltonian* can be represented as

$$H_B^f = -\sum_{\langle ij\rangle,\sigma} J_{ij}^f c_{i\sigma}^\dagger c_{j\sigma} + \text{H.c.} + \sum_i U_i^f n_{i\uparrow} n_{i\downarrow}. \quad (1)$$

Here J_{ij}^f is the hopping strength between sites i and j, where $\langle ij\rangle$ indicates that only the nearest-neighbor hopping is allowed, and U_i^f denotes the on-site interaction at the site i of the lattice, occupied by fermions, which can be repulsive as well as attractive. $c_{i\sigma}$ ($c_{i\sigma}^\dagger$) is the fermionic annihilation (creation) operator obeying the canonical anticommutation relations, $\{c_{i\sigma}, c_{j\sigma'}^\dagger\} = \delta_{ij}\delta_{\sigma\sigma'}$, $\{c_{i\sigma}, c_{j\sigma'}\} = 0$, and $\{c_{i\sigma}^\dagger, c_{j\sigma'}^\dagger\} = 0$, and $n_{i\sigma} = c_{i\sigma}^\dagger c_{i\sigma}$ is the number operator on site i with spin σ.

Instead of fermions, when the lattice sites are filled with bosons, the *Bose-Hubbard Hamiltonian* reads

$$H_B^b = -\sum_{\langle ij\rangle} J_{ij}^b b_i^\dagger b_j + \text{H.c.} + \sum_i \frac{U_i^b}{2} n_i(n_i - 1), \quad (2)$$

where J_{ij}^b and U_i^b are the hopping strength from site i to j and the on-site interaction strength at the ith site, respectively, and b_i ($b_i^\dagger$) is the bosonic annihilation (creation) operator following the standard canonical commutation relations for bosons. For both models, we consider the open boundary condition. Moreover, from now on, site-independent parameters will be denoted without the subscripts i and j, thereby representing the ordered models.

Charging. In order to charge the system, we construct the charging Hamiltonian for fermions and bosons, respectively, as

$$H_c^f = U_c^f \sum_i n_{i\uparrow} n_{i\downarrow}, \quad H_c^b = \frac{U_c^b}{2} \sum_i n_i(n_i - 1). \quad (3)$$

Here U_c^μ is the charging strength, and in general, $U_c^\mu \neq U^\mu$. The reason for choosing such a form of the charging Hamiltonian is threefold. First, we choose the charging Hamiltonian in such a way that the evolution is nontrivial. Precisely, the charging Hamiltonian should not commute with the battery Hamiltonian; otherwise, the system cannot evolve. To ensure this, we put $J^\mu = 0$ in the original Hamiltonian and construct the charging Hamiltonian with a different charging strength, denoted by U_c^μ, which is, in general, not equal to U^μ ($\mu =$ f or b) of the battery Hamiltonian H_B^μ. Second, a charging Hamiltonian with $J \neq 0$ and $U = 0$ represents a global charging which we do not wish to analyze since the extra increment in power can happen due to the global charging in the system. Finally, from an experimental point of view, adjusting U is much easier than controlling the other parameters of the system. In an ultracold-atom setup, the intensity can be tuned just by a "control knob," as demonstrated in Refs. [65–67]. For example, the ratio U/J can be tuned by the laser intensity which regulates the lattice potential depth s. Tuning the corresponding s is the way to traverse the quantum phase transition, i.e., between Mott and superfluid phases. In the design discussed above, the battery should be charged with the Bose- (Fermi-) Hubbard model with $J = 0$, i.e., quenched in the Mott-insulator phase. Specifically, when $s > 13E_r$ [66], the system is in the Mott-insulator phase, where $E_r = h/8md^2$, with m being the atomic mass, $d = 406$ nm being the lattice spacing, and h being Planck's constant. The value of s can be dynamically modulated to perform the quench without having any restriction on the timescale for the quench, and hence, one can expect that the charging of the battery can be achieved in a similar experiment.

Quantifying performance. By employing unitary operations, $\mathcal{U}_c = \exp(-iH_c^\mu t)$, such that $\rho(t) = \mathcal{U}_c\rho(0)\mathcal{U}_c^\dagger$, with $\rho(0)$ being the initial state of the QB, the total amount of energy that can be stored and extracted from the QB (the work output) at time t reads

$$W^\mu(t) = \text{Tr}\big[H_B^\mu \rho(t)\big] - \text{Tr}\big[H_B^\mu \rho(0)\big], \quad (4)$$

where the first and second terms in Eq. (4) are the final and initial energies of the system, respectively. Notice that the maximum amount of extractable work from the quantum battery in terms of ergotropy coincides with the above equation in the case of a reversible unitary process. This is due to the fact that for entropy-preserving unitary operations, the maximum amount of extractable work is equal to ergotropy [68,69]. Note, moreover, that the stored energy, in general, does not coincide with the extractable work (ergotropy) when the battery Hamiltonian is in contact with the environment [28–32,34].

The maximum average power output from the battery at time t is quantified as

$$P_{\max}^\mu = \max_t \frac{W^\mu(t)}{t}. \quad (5)$$

Throughout the paper, we will use $P_{\max}^\mu$ as the figure of merit for determining the performance of the QB. Notice also that $P_{\max}^\mu = 0$ when the hopping term of the QB vanishes. It is important to note that the charging Hamiltonian is turned on when $t > 0$, and hence, the energy cost of turning the charging Hamiltonian on and off is typically not considered during the computation of power.

Scaling. By increasing the values of U_i^μ and J_i^μ ($\mu = f, b$) of H_B^μ, it is possible to store more and more extractable power output from the quantum battery, which makes the analysis trivial. To avoid such an undesirable situation, we normalize the Hamiltonian in such a way that its spectrum is bounded by $[-1, 1]$, irrespective of any system parameters, including the system size. In addition, since we compare two different models, namely, FH and BH, it is necessary to consider them on equal footing from the perspective of energies, which can also be taken care of by the normalization. Hence, the normalized Hamiltonians reads

$$\frac{1}{E_{\max} - E_{\min}}\big[2H_B^\mu - (E_{\max} + E_{\min})\mathbb{I}\big] \to H_B^\mu, \quad (6)$$

where $E_{\max}$ and $E_{\min}$ are the maximum and minimum eigenvalues of H_B^μ. Here since the evolution is unitary, the excitation spectrum is also conserved in both cases, which also ensures that the comparison is fair.

III. PERFORMANCE OF A QB FOR AN ARBITRARY NUMBER OF LATTICE SITES: COMPARING BOSONS WITH FERMIONS

Let us now concentrate on a hierarchy among QBs based on BH and FH models according to their performance. We start with two lattice sites and then investigate the trends of

the power output for arbitrary lattice sites. In this section, the number of particles is the same as the number of lattice sites.

A. Two lattice sites: Equivalence between bosonic and fermionic systems

First, consider a scenario in which two particles occupy a lattice with two sites. In this situation, the work output can be found analytically for both bosons and fermions, and their relation is as follows.

Proposition 1. The average work outputs for BH and FH models coincide for a lattice with two sites occupied by two particles if the values of on-site interactions, hopping, and charging strengths are identical and the initial state of the battery is prepared as the ground state of the Hamiltonian.

Proof. The two-site Fermi-Hubbard model occupied by two fermions has four basis states. Generically, the Fock-state bases are defined as $|x_1y_2\rangle_\uparrow|z_1w_2\rangle_\downarrow$. Here $\{x_1, y_2, z_1, w_2\} \in (0, 1)$, where 0 denotes the situation when the lattice site is not occupied by fermions, while 1 indicates when the fermion occupies the lattice site and subscripts denote the lattice sites, which we drop from now on; we will use only the binary method to indicate the entire configuration. In this basis, the normalized Hamiltonian reads

$$H_B^f = \frac{1}{\sqrt{16J^{f2} + U^{f2}}} \begin{bmatrix} U^f & -2J^f & -2J^f & 0 \\ -2J^f & -U^f & 0 & -2J^f \\ -2J^f & 0 & -U^f & -2J^f \\ 0 & -2J^f & -2J^f & U^f \end{bmatrix},$$

while the ground state H_B^f as the initial state of the battery is given by

$$\rho(0) = \begin{bmatrix} \frac{1}{4}(1-a) & b & b & \frac{1}{4}(1-a) \\ b & \frac{1}{4}(1+a) & \frac{1}{4}(1+a) & b \\ b & \frac{1}{4}(1+a) & \frac{1}{4}(1+a) & b \\ \frac{1}{4}(1-a) & b & b & \frac{1}{4}(1-a) \end{bmatrix}, \tag{7}$$

where $a = \frac{U^f}{\sqrt{16J^{f2}+U^{f2}}}$ and $b = \frac{J^f}{\sqrt{16J^{f2}+U^{f2}}}$. The charging Hamiltonian in the Fock basis reduces to

$$H_c^f = U_c^f(|1010\rangle\langle 1010| + |0101\rangle\langle 0101|), \tag{8}$$

which is used up to a certain time t to charge the battery, resulting in an evolved state,

$$\rho(t) = \begin{bmatrix} \frac{1}{4}(1-a) & be^{-itU_c^f} & be^{-itU_c^f} & \frac{1}{4}(1-a) \\ be^{itU_c^f} & \frac{1}{4}(1+a) & \frac{1}{4}(1+a) & be^{itU_c^f} \\ be^{itU_c^f} & \frac{1}{4}(1+a) & \frac{1}{4}(1+a) & be^{itU_c^f} \\ \frac{1}{4}(1-a) & be^{-itU_c^f} & be^{-itU_c^f} & \frac{1}{4}(1-a) \end{bmatrix}. \tag{9}$$

The work output in this case simplifies to

$$W^f(t) = \frac{J^{f2}}{J^{f2} + \frac{(U^f)^2}{16}}\left[1 - \cos\left(tU_c^f\right)\right]. \tag{10}$$

Following the same prescription, we also calculate (for a detailed calculation, see Appendix A) the total work output considering the BH model for the same time interval t,which is given by

$$W^b(t) = \frac{J^{b2}}{J^{b2} + \frac{(U^b)^2}{16}}\left[1 - \cos\left(tU_c^b\right)\right]. \tag{11}$$

Hence, if $J^f = J^b$, $U^f = U^b$, and $U_c^f = U_c^b$, the average work outputs in both cases are the same. ■

Remark 1. Although different numbers of basis states appear due to exchange symmetry for different spin statistics for both fermions and bosons, the design of the charging Hamiltonian is responsible for the equal work output obtained in Proposition 1 for two lattice sites. As mentioned before, the charging Hamiltonian acts on only those lattice sites that consist of at least two particles and the number of such states having two particles on a single site occurs an equal number of times in both bosonic and fermionic batteries, which leads to the equal work output from the battery. In the succeeding sections, we report unequal power from bosonic and fermionic batteries for a large number of lattice sites.

B. Arbitrary number of lattice sites: Bosons vs fermions

Let us now move further and consider a lattice with more than two sites. First, we consider three sites occupied by three particles, bosons or fermions. Unlike the previous case, we establish a hierarchy between the performance of the batteries with bosons and with fermions.

Proposition 2. The battery composed of three lattice sites filled with three fermions is better in terms of the work output than that of bosonic systems in the absence of on-site interaction of the battery Hamiltonian, provided the charging strengths of the on-site interactions for both fermions and bosons are the same, i.e., $U_c^f = U_c^b = U_c$.

Proof. Following the same procedure (see Appendix B) as in the previous proof, we calculate $W^f(t)$ and $W^b(t)$ for a lattice with $L = 3$, occupied by three fermions and three bosons, governed by FH and BH, respectively, with $U^\mu = 0$, $\mu = f, b$. If the values of the charging strength for both cases are identical, the difference in the work output turns out to be

$$W^f(t) - W^b(t) = 0.13[1 - \cos(tU_c)], \tag{12}$$

which is positive and hence the proof. Note here that the output work is independent of any system parameters since the Hamiltonian is normalized and the spectrum is bounded between -1 and 1, which allows us to compare two different models on the same footing. Since $U^\mu = 0$, the expression for the Hamiltonian involves only J^μ, which gets canceled after the normalization. Moreover, the normalization is also responsible for the prefactor 0.13 in Eq. (12) [compare Eqs. (B2) and (B4)]. ■

Proposition 2 indicates that the increasing value of the lattice size and the number of particles can have significant effects on the power output for these two models. In particular, identifying the parameter range where the FH battery outperforms the BH one can be an interesting question to address with $L \geqslant 3$. Towards that aim, the initial battery state is considered to be the ground state of the FH lattice filled with

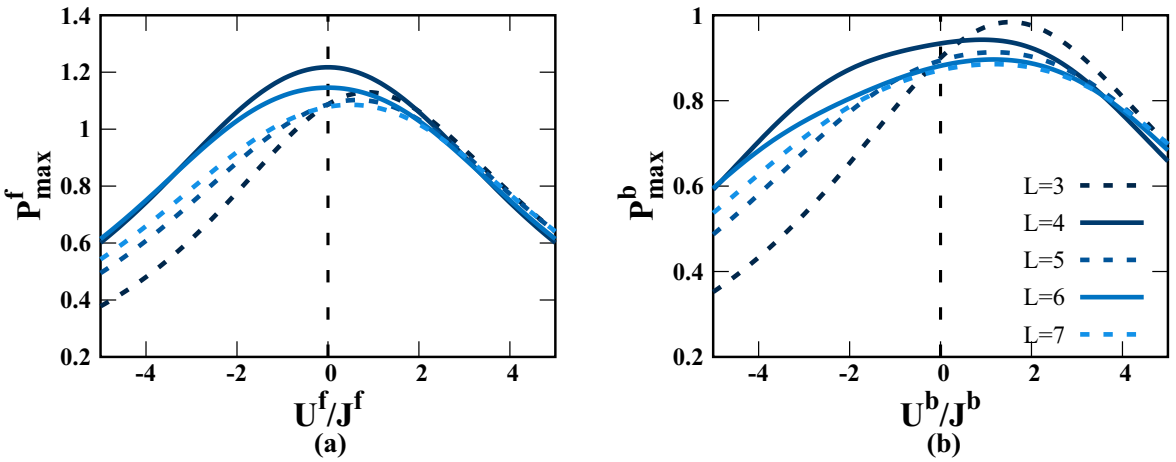

FIG. 2. (a) Power output $P^f_{\max}$ (ordinate) with respect to U^f/J^f (abscissa) of the battery constructed via the Fermi-Hubbard model. (b) $P^b_{\max}$ (ordinate) versus U^b/J^b (abscissa) for bosonic systems. The system is half filled in both cases, and the initial state of the battery is the ground state of the system. In the case of the Bose-Hubbard model, at most two bosons per sites are allowed. The charging of the battery is performed by using on-site interaction, with the strength being $U^f_c = U^b_c = 2$. Solid lines correspond to an even number of lattice sites L, while the dashed lines represent odd L. In both cases, dark to lighter shades indicate the increase of L. Both axes are dimensionless.

$N^f_\uparrow = \lfloor L/2 \rfloor + L(\mathrm{mod}\,2)$ and $N^f_\downarrow = \lfloor L/2 \rfloor$ fermions, where the total number of fermions $L = N^f = N^f_\uparrow + N^f_\downarrow$, while the BH battery is occupied by $N^b = L$ bosons with two particles per site, i.e., a single site can be occupied by at most two bosons; the distribution of fermions and bosons in this way is called half filling. We will lift the restriction of particles per site in the next section. In the rest of the paper, we carry out our analysis of $P^\mu_{\max}$ by varying U^μ/J^μ ($\mu = f, b$) since the various phases like Mott insulators, superfluids, Fermi liquids, and quantum phase transitions can successfully be described by the different limits of this ratio. Moreover, in the entire calculation, we take the strength of the charging field to be $U^f_c = U^b_c = 2$. Notice, however, that with the increase of the charging on-site interactions, the power gets enhanced. It can also be understood from the expressions of work in Eqs. (10), (11), and (12), which clearly show that the maximum power is obtained for small time when one increases U^μ_c.

Contrasting trends for FH and BH batteries. The patterns of $P^\mu_{\max}$ with U^μ/J^μ for a paradigmatic example of half filling of lattice sites for both fermions and bosons are depicted in Fig. 2, and we observe that contrasting behaviors emerge for bosons and fermions. (1) The FH-based battery produces more power output than that of the BH model in almost the entire range of U^μ/J^μ. We will determine the exact range of the advantage obtained via fermionic systems in Figs. 3–5, which we will discuss later. (2) In the case of an even number of lattice sites with the FH model, $P^f_{\max}$ is symmetric about the $U^f/J^f = 0$ line, thereby leading to maximum average power output with $U^f = 0$, although no such symmetry is observed in the case of bosons. (3) In the half-filling regime, among all the lattice sites considered, i.e., when $3 \leqslant L \leqslant 7$, we find that $P^f_{\max}$ reaches its maximal value for $L = 4$, while $P^b_{\max}$ shows a maximum with $L = 3$ and $U^b/J^b > 0$. Although there is, in general, no visible correlation between lattice size and higher work output, $P^\mu_{\max}$ converges to a certain value for all values of L in the presence of strong repulsive and attractive interactions, thereby illustrating a site-independent power output.

To compare the batteries constructed with fermionic and bosonic systems, we introduce a quantity which we call the performance score,

$$\Delta^{f-b}_P = P^f_{\max} - P^b_{\max},$$

by fixing $U^f = U^b = U$ and $J^f = J^b = J$. From Fig. 3, we observe that when $-5 \lesssim U/J < 0$, i.e., with attractive on-site interactions, FH batteries can always store (extract) more energy than BH batteries, although the situation changes when $U/J \gtrsim 3$. Specifically, there exists a critical U/J value $(U/J)_{\text{critical}}$ above which bosonic systems can produce more power than that of fermionic systems, i.e., $\Delta^{f-b}_P < 0$ when $U/J > (U/J)_{\text{critical}}$. We also notice that $(U/J)_{\text{critical}}$ depends on L, as shown in Fig. 4, which indicates that with the increase of L, a higher on-site interaction is required to achieve a higher power when using the BH model compared with that of the FH one.

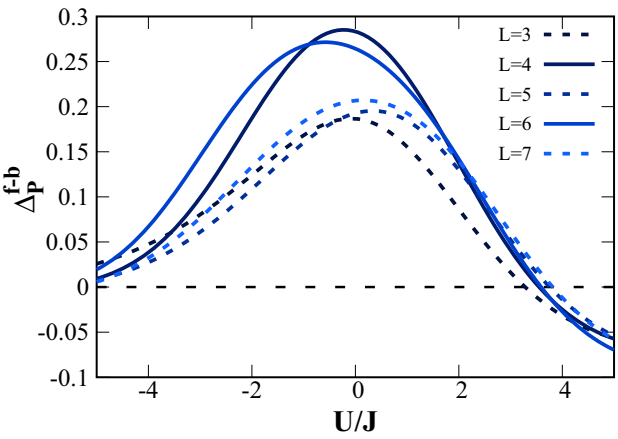

FIG. 3. Bosonic vs fermionic QBs. Performance score $\Delta^{f-b}_P = P^f_{\max} - P^b_{\max}$ (vertical axis) against $U/J = U^b/J^b = U^f/J^f$ (horizontal axis). All other specifications are the same as in Fig. 2. Both axes are dimensionless.

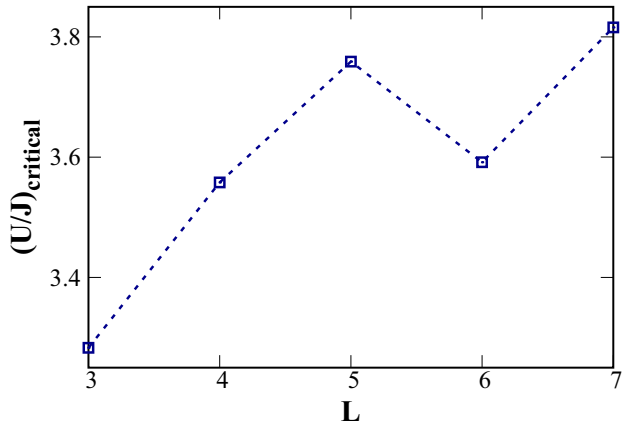

FIG. 4. Scaling of the hierarchy. The critical value of U/J, denoted by $(U/J)_{\text{critical}}$ (y axis), above which the batteries built with the BH model can store more energy than those of the FH model with respect to lattice sites L (x axis). All the axes are dimensionless.

If one increases the value of on-site interaction, the system undergoes a phase transition from the superfluid phase to the Mott-insulator one; that is, the probability of hopping between the lattice sites decreases and becomes vanishingly small at some point. Moreover, due to the half-filled scenario, all the lattice sites then contain only one particle effectively, and due to the design of the charging Hamiltonian, the excitation in the system becomes minimal, resulting in a very low power output from the battery. This implies that the difference in the output power between FH and BH systems also goes to zero (see Fig. 5) since at a very high value of U/J, the power output from the individual system also vanishes. In other words, in an extreme scenario, when both the charging and battery Hamiltonian are in the Mott-insulating phase, i.e., when $U \gg J$, the battery cannot be charged, while moderate values of U/J are favorable for storing the power in the battery, as also shown in Fig. 5.

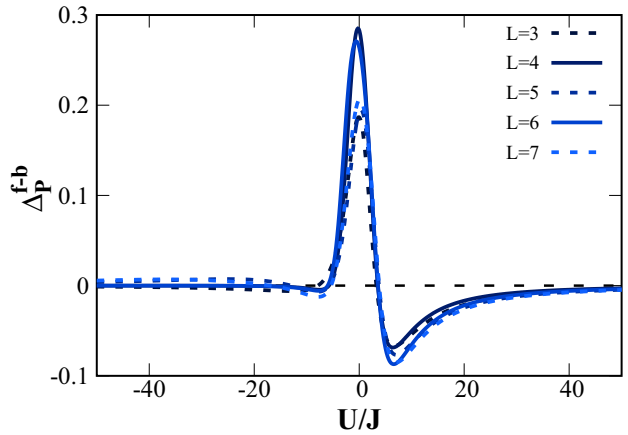

FIG. 5. Comparison between fermionic and bosonic QBs with high U/J values. $\Delta_P^{f-b} = P_{\max}^f - P_{\max}^b$ (ordinate) vs $U/J = U^b/J^b = U^f/J^f$ (abscissa). All other specifications are the same as in Fig. 2. Note that for high U/J values, power vanishes in both cases, thereby leading to the vanishing performance score. Both axes are dimensionless.

$(U/J)_{\text{critical}}$ and the energy distribution. In order to explain the $(U/J)_{\text{critical}}$ value, we check the energy distribution of the state that produces maximum average power. More precisely, we calculate the inner product between the evolved state giving the maximum power and eigenstates of the corresponding Hamiltonian; that is, if the state that stores the maximum average power is $|\psi^\mu(t)\rangle$ ($\mu = f, b$), we compute the quantity $p_i^\mu = |\langle \epsilon_i^\mu | \psi^\mu(t)\rangle|^2$, where $|\epsilon_i^\mu\rangle$ is the eigenstate of the BH or FH model with energy E_i. To identify the dynamically preferred state, we compute the energetically preferred distribution as

$$\left\{ED_i^\mu\right\} = \left\{p_i^\mu E_i^\mu\right\} \ \forall \ i = \left\{1 \cdots N_E^\mu\right\}, \tag{13}$$

where N_E^μ is the number of eigenvectors $\{|E_1^\mu\rangle, |E_2^\mu\rangle, \ldots, |E_{N_E}^\mu\rangle\}$ in both the Bose and Fermi cases. We study $\{ED_i^\mu\}$ against the corresponding $\{E_i\}$ in Fig. 6. It shows that when U^μ/J^μ ($\mu = f, b$) is less than the critical point where the fermionic battery is better than the bosonic ones, there is a larger energetic contribution from the excited state in the Fermi case compared to the bosonic ones. After the critical point, the situation reverses, and the excited states in the Bose-Hubbard model contribute more than those in the Fermi-Hubbard case.

IV. EFFECTS OF THE FILLING FACTOR AND TEMPERATURE ON THE AVERAGE POWER OUTPUT

Until now, the entire analysis has been carried out by considering the half filling and the case when the battery is the ground state of the Hamiltonian. Let us lift both restrictions and study the consequences for the performance of the QB.

First, we explore the dependence of *filling factors* on the power output of the battery. Before going further, let us first discuss two extreme situations for which the power outputs vanish when the battery is made of *fermions*.

Remark 2. For a fixed lattice site, if all the lattice sites are completely occupied by up or down or both up and down fermions allowed by the Pauli exclusion principle, no work can be extracted from the system since no excitation is possible in this scenario.

Remark 3. Suppose all the lattice sites are filled with down (up) fermions. If we now increase the number of up (down) fermions one by one on a lattice, the power output again vanishes. This is because in this process, the charging Hamiltonian comes out to be an identity matrix multiplied by a constant, which is the strength of the charging field, and after evolving for a time interval t, the evolved state $\rho(t)$ remains identical to the initial ground state $\rho(0)$. Hence, to obtain a nontrivial power output from the QB, the number of up and down fermions in the system of L lattice sites must be upper bounded by $L-1$.

In the fermionic system, we also find the following:

Observation 1. The *maximum extractable power* is the same under the exchange of the total number of up and down fermions in the system, i.e., $P_{\max}(N_\uparrow^1, N_\downarrow^2) = P_{\max}(N_\downarrow^1, N_\uparrow^2)$, where N^i, $i = 1, 2$, is the number of up (down) and down (up) fermions, respectively. Moreover, we notice that $P_{\max}(N_\uparrow^1, N_\downarrow^2) = P_{\max}(L - N_\uparrow^1, L - N_\downarrow^2)$.

Following all these symmetries, let us first calculate the number of configurations that give the nontrivial dynamics

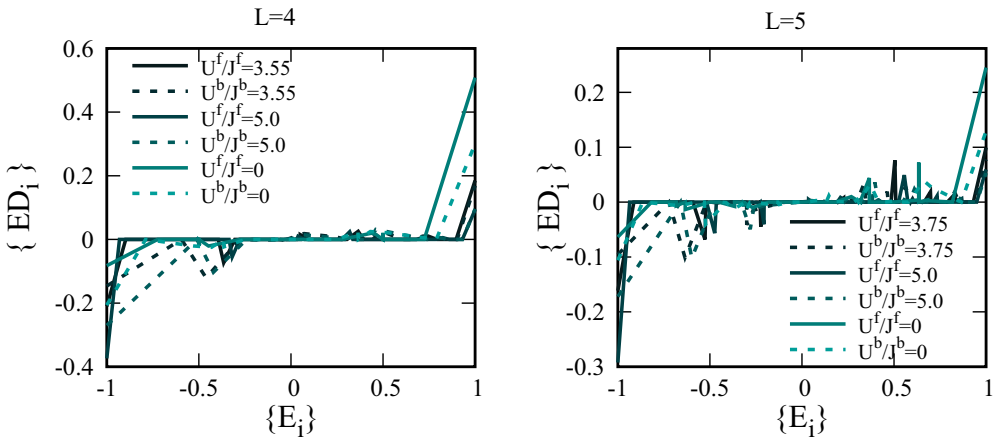

FIG. 6. $\{ED_i\}$ against the corresponding energy eigenvalues of the normalized Hamiltonian $\{E_i\}$ for two different lattice sites, $L = 4$ (left) and $L = 5$ (right). Here $U_c = 2$. Solid (dashed) lines correspond to fermions (bosons). With the increase of U^μ/J^μ, the shades get lighter. Both axes are dimensionless.

of a fermionic system with a total number of lattice sites L. The constraints which dictate the configurations are given by (1) $N_\uparrow^1 + N_\downarrow^2 \leqslant L$, (2) $N_\uparrow^1, N_\downarrow^2 \geqslant 1$, and (3) $N_\uparrow^1, N_\downarrow^2 := L - N_\uparrow^1, L - N_\downarrow^2$. Therefore, the total number of configurations $\mathcal{S}$ contributing to the output power is given by

$$\mathcal{S} = (L-1) + \{(L-2)-1\} + \cdots + \left\{\left(L - \left\lfloor \frac{L}{2} \right\rfloor\right) - \left\lfloor \frac{L}{2} \right\rfloor + 1\right\}. \tag{14}$$

It is easy to check that for even L, $\mathcal{S} = \frac{L^2}{4}$, while $\mathcal{S} = \frac{L^2-1}{4}$ when L is odd. For example, with $L = 2$, the total number of possible configurations is seven. However, incorporating all the aforementioned symmetries, we observe that only a particular configuration among all those choices is responsible for the maximum amount of power from the battery, which turns out to be $N_\uparrow^f = 1$ and $N_\downarrow^f = 1$ for the entire parameter regime of U^f/J^f as counted in Eq. (14). However, by increasing the lattice sites, we obtain the maximum power contribution from different filling factors depending on the tuning parameter U^f/J^f. To capture it, we introduce a quantity $\widetilde{P}^f_{\max} = \max P^f_{\max}$ (see Fig. 7) where the maximization is performed over all possible configurations. First of all, $\widetilde{P}^f_{\max}$ decreases with the increase of lattice sites, although the rate of decrease depends on whether L is even or odd. Second, the average power output is symmetric about $U^f/J^f = 0$ (compared with Fig. 3). Third, unlike for an even number of lattice sites, the value of $\widetilde{P}^f_{\max}$ is independent of L at $U^f/J^f = 0$ for an odd number of lattice sites, although the maximum occurs at some point with $U^f/J^f > 0$ and $U^f/J^f < 0$ symmetrically.

In the case of the BH model, we consider a scenario in which the number of lattice sites is fixed to L and available particles per site is at most n. Again, we examine $\widetilde{P}^b_{\max} = \max P^b_{\max}$, where the maximization is taken over all the allowed configurations possible under the constraint of n particles per site, thereby optimizing over nL configurations (see Fig. 8 for $L = 4$). For a fixed number of lattice sites, $\widetilde{P}^b_{\max}$ increases with the increase of n. In contrast to the fermionic battery, the power output for the bosonic battery is not symmetric about the $U^b/J^b = 0$ line.

Role reversal of bosonic and fermionic batteries depending on temperature. In a more realistic situation, one expects that the initial state of the quantum battery is the thermal state or the canonical equilibrium state (ρ_{th}) of the Hamiltonian. To illustrate the effects of temperature on the maximum average power output of the battery built using the BH and FH models, we examine the performance score Δ_P^{f-b} by varying U/J, where $U^b = U^f = U$ and $J^f = J^b = J$, and we set $\beta = |J|\beta'$. With the increase of temperature, we find that Proposition 1 for two lattice sites does not remain valid, i.e., $P^f_{\max} \neq P^b_{\max}$ with some moderate temperature. Specifically, we find that for $U/J = 5$, Δ_P^{f-b} becomes negative when the initial state is prepared at $\beta \lesssim 39.5$, thereby showing that bosonic batteries outperform the fermionic ones. Such an advantageous role of bosonic systems persists also for a higher number of lattice sites with a certain β value and a wide range of U/J, as depicted in Fig. 9. Specifically, if the initial state is prepared at

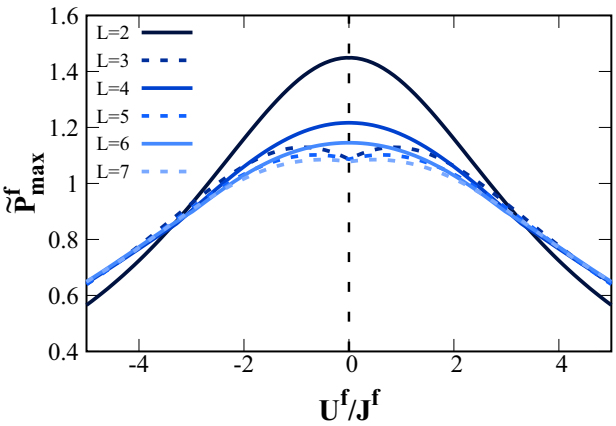

FIG. 7. Variation of $\widetilde{P}^f_{\max}$ (see the text for the definition; ordinate) vs U^f/J^f (abscissa). Notice that the symmetry missing around the $U^f/J^f = 0$ line in Fig. 2 for odd lattice sites can be attained by considering the quantity $\widetilde{P}^f_{\max}$ obtained after maximizing over configurations. All other specifications are the same as in Fig. 2. Both axes are dimensionless.

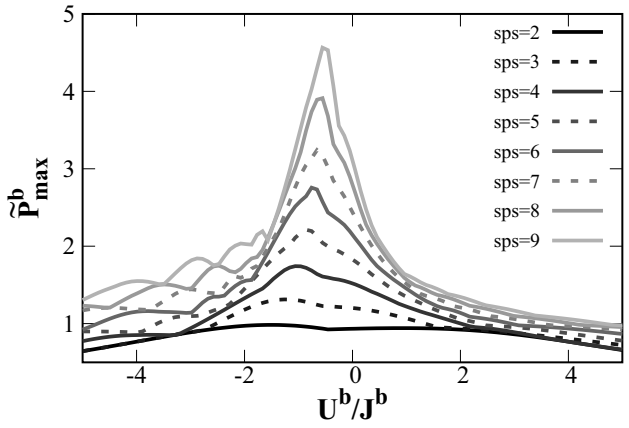

FIG. 8. $\widetilde{P}^b_{\max}$ (vertical axis) vs U^b/J^b (horizontal axis) for the BH model-based battery. Solid and dashed lines correspond to even and odd values of states per site (sps), respectively, which can reach at most n. Here $L = 4$. The optimization involved in $\widetilde{P}^b_{\max}$ is performed over all nL configurations. Dark to lighter shade indicates the increase of state per site. All axes are dimensionless.

a very high temperature, the maximum average power output obtained from the BH model is higher than that of the FH one for most of the repulsive on-site interactions, i.e., for positive values of U/J.

V. ROBUSTNESS OF BATTERIES BASED ON HUBBARD MODELS IN THE PRESENCE OF DISORDER

In an ultracold-atom experiment, disorder can be introduced in the system in a controlled manner [37], leading to the quenched disordered system. In particular, van der Waals losses are mitigated by placing atoms at a significant distance from the atom chip, which results in an adjustment of the magnetic wire, leading to the uniform disorder in the on-site intraparticle interactions U^μ/J^μ ($\mu = f, b$) [70,71] of the Hubbard Hamiltonian. The disorder is chosen from a uniform distribution, $U^\mu_u/J^\mu \in [a, b]$, with mean $\langle U^\mu_u\rangle/J^\mu = \frac{a+b}{2}$ and

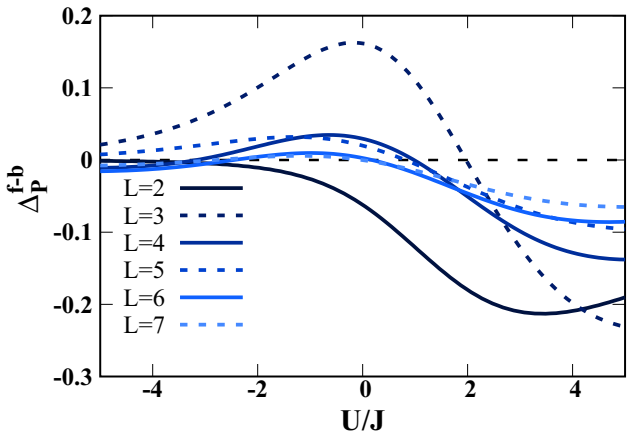

FIG. 9. Δ^{f-b}_P (vertical axis) with U/J (horizontal axis). Here $\beta = 3$. All other specifications are the same as in Fig. 2. All axes are dimensionless.

standard deviation $\sigma^\mu_u = \sqrt{\frac{(b-a)^2}{12}}$. On the other hand, the local potential can also be sampled from the Gaussian distribution [72], $U^\mu_G/J \in \frac{1}{\sigma^\mu_G\sqrt{2\pi}} e^{-\frac{1}{2}(\frac{x-\langle U^\mu_G\rangle/J^\mu}{\sigma^\mu_G})^2}$, with mean $\langle U^\mu_G\rangle/J^\mu$ and standard deviation σ^μ_G. Here the subscripts u and G in the mean and standard deviation represent the uniform and Gaussian distributions, respectively.

By incorporating uniform and Gaussian randomness in the on-site interactions $\langle U^\mu_u\rangle/J^\mu$ and $\langle U^\mu_G\rangle/J^\mu$ of the batteries built using the FH and BH models, we examine the quenched maximum average power [73] $\langle P^\mu_{\max}\rangle$. It is obtained by computing $P^\mu_{\max}$ for every value of U^μ/J^μ chosen randomly from both uniform and Gaussian distributions with the corresponding means and standard deviations. The number of realizations considered here for calculations is 2×10^5, leading to a convergence up to two decimal places. In order to maintain a fair comparison between systems with and without disorder, we choose $L = 4$ sites with half filling; the particles per site for bosons are restricted to two, while the numbers of spin-up and spin-down fermions are the same. We report that for both bosons and fermions, $\langle P^\mu_{\max}\rangle$ does not change substantially in the presence of impurities in the on-site interactions, as shown in Fig. 10(a), thereby illustrating robustness in the performance of the battery against disorder.

On the other hand, disorder in the hopping parameter of the Hubbard Hamiltonian can be realized by modulating the applied electric field of the laser or by doping impurities in the system [72,74]. In this scenario, the quenched disorder power outputs $\langle P^\mu_{\max}\rangle$ from the FH and BH models are again computed by varying $\langle J^\mu_{G(u)}\rangle/U^\mu$ for different but fixed standard deviations. Like randomness in the on-site interactions, when both uniform and Gaussian disorders are impinged in the hopping terms of the Bose- and Fermi-Hubbard Hamiltonians, thereby changing the initial state of the battery, no significant consequences for the power of the battery are observed over the ordered case [see Fig. 10(b)]. Interestingly, however, when we do a close inspection, we notice that for $\langle J^\mu_G\rangle/U^\mu < 0.15$ ($\langle J^\mu_u\rangle/U^\mu < 0.15$), the quenched averaged power output from the disordered battery is higher than that of the ordered case, thereby showing improvements in the performance of the battery in the presence of impurities in the hopping. Such a *disorder-enhanced power* is discovered for both fermionic and bosonic systems. In the ordered scenario with $\sigma = 0$ in Figs. 10(c) and 10(d), the output power is a monotonically increasing function of J^μ, i.e., $J^\mu(\epsilon) > J^\mu(\epsilon')$ where $\epsilon > \epsilon'$ in some parameter regime. Moreover, it has a very high slope in the same parameter regime, which implies that $\langle P^\mu_{\max}\rangle(\langle J^\mu\rangle_{i+1}) - \langle P^\mu_{\max}\rangle(\langle J^\mu\rangle_i) \gg \langle J^\mu\rangle_{i+1} - \langle J^\mu\rangle_i$ around $J^\mu = \epsilon$ with $\epsilon \to 0$. By introducing disorder into the system, we perform averaging over different realizations of J^μ from a range of $\eta + 3\sigma$ to $\eta - 3\sigma$ in the parameter space, where η is the mean value of J^μ and σ is the standard deviation. Since there are parameter values of J^μ where the slope of the power with $\sigma = 0$ is much higher than unity, the power obtained between $[\eta, \eta + 3\sigma]$ is much higher than that obtained in the region with $[\eta - 3\sigma, \eta]$, thereby providing higher power values for the disordered case than for the ordered ones. Specifically, the advantage in power with impurities is detected in the regime $0 \leqslant \langle J^b_u\rangle/U \leqslant 0.12$ for bosons, while

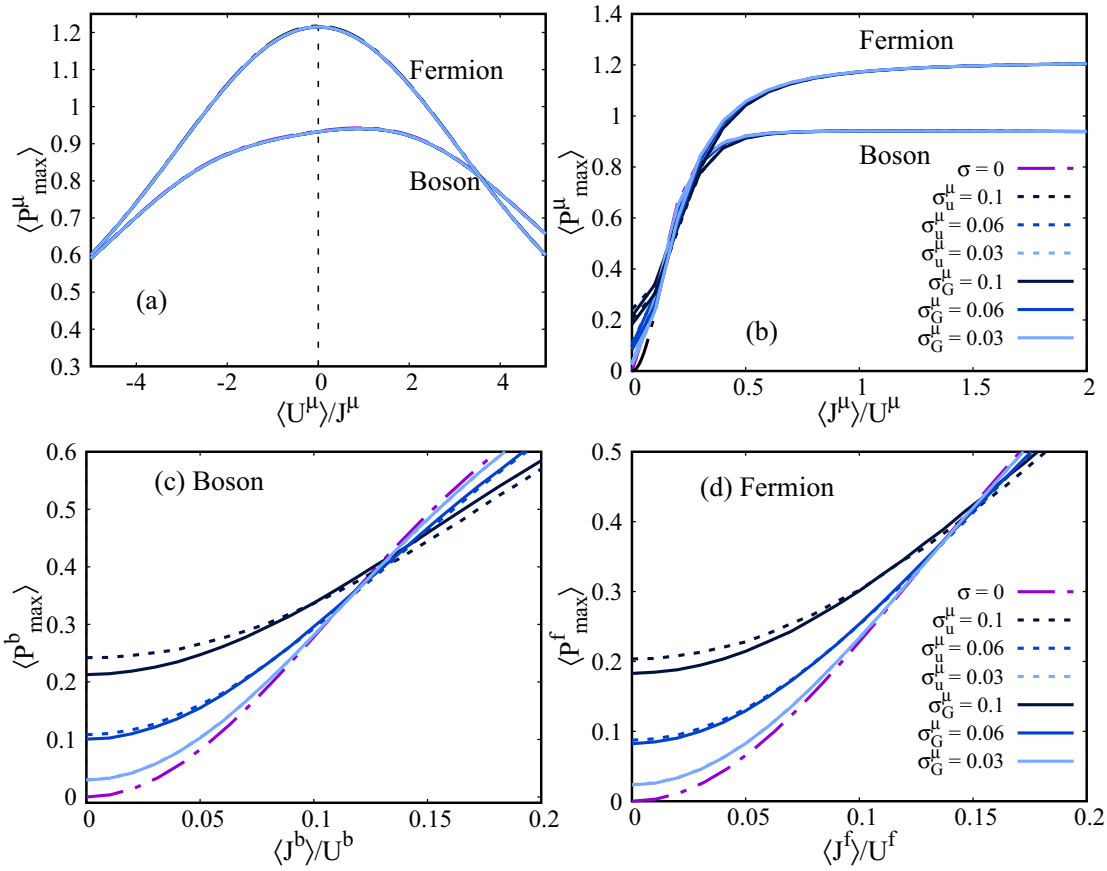

FIG. 10. Disorder-enhanced power. (a) and (b) Quenched averaged power $\langle P^{\mu}_{\max}\rangle$ by varying $\langle U^{\mu}\rangle/J$ and $\langle J^{\mu}\rangle/U$ with $\mu = f, b$. Here $L = 4$, and the initial state is the ground state of the system. σ^{μ}_{G} and σ^{μ}_{u} represent the standard deviations of the Gaussian (solid line) and uniform (dashed line) distributions, respectively, from which the on-site interactions and the hopping are randomly chosen. Note that $\sigma = 0$ represents the ordered systems (dash-dotted line). Higher $\langle P^{\mu}_{\max}\rangle$ values correspond to the disordered FH models, while the lower values are for the bosonic systems. (c) and (d) $\langle P^{b}_{\max}\rangle$ and $\langle P^{f}_{\max}\rangle$ are plotted with respect to $\langle J^{b}\rangle/U$ and $\langle J^{f}\rangle/U$, respectively. Dark to lighter shade indicates the decrease of standard deviation, except for the ordered case. In both situations, systems with impurities turn out to be a better storage device than that of ordered systems, thereby showing disorder-induced power. All axes are dimensionless.

the range of parameters $\langle J^{f}_{u}\rangle/U \in [0, 0.148]$ increases in the case of the FH model [compare Figs. 10(c) and 10(d)]. Note, interestingly, that the power obtained in the disordered case is almost equal to the battery with the ordered Hamiltonian in the entire range of parameters, thereby establishing the robustness against impurities in such a battery design.

VI. CONCLUSION

Batteries are integral parts of any technology for storing power and utilizing it as a source of energy at any point in time. We know that the existing batteries that we termed classical batteries convert chemical energy to electrical energy and are quite useful, although current technological developments demand miniaturization, which inevitably has the possibility of entering the quantum regime. To fulfill the requirements, quantum technologies are designed which also necessitate the modeling of a storage device based on quantum mechanics, leading to quantum batteries. Recently, several experimental proposals for QBs using quantum dots coupled to cavities, superconducting qubits, have been developed and realized.

In this work, we designed a quantum battery in the presence and absence of impurities using ultracold atoms in optical lattices which can be implemented via currently available technologies. In particular, we prepared the initial state of the quantum battery as the ground or thermal state of the Fermi-Hubbard and Bose-Hubbard models. The charging process of the battery was carried out by tuning the on-site interactions. We showed that in the case of more than two lattice sites and with half filling, the QB based on the Fermi-Hubbard model can store a larger amount of energy compared to the battery based on the Bose-Hubbard model provided the on-site interactions are attractive or repulsive with moderate values. The situation is reversed if the temperature in the initial state is reasonably high. Moreover, we noticed that the filling factors in both bosonic and fermionic models play a crucial role in the power output of the battery. Specifically, the maximum average power after optimizing over all the configurations increases with the increase of particles per site in the case of bosons.

One of the success stories in ultracold atomic systems is the realization of disorder in a controlled manner. We found that the randomness in the uniform and Gaussian distributions in the hopping and in the on-site interactions does not affect the performance of the QB significantly, thereby demonstrating the advantage of preparing these batteries based on

ultracold atoms. We also identified a region of mean hopping strength below which the quenched averaged power is higher for the disordered system than for the ordered ones: disorder-enhanced power. The engineering of QBs proposed via bosonic and fermionic systems opens up the possibility to design thermal machines based on Hubbard models that are realizable in laboratories, and at the same time, it can pinpoint the regime in which machinery based on bosons is better than that based on fermions and vice versa.

ACKNOWLEDGMENTS

We acknowledge support from the Interdisciplinary Cyber Physical Systems (ICPS) program of the Department of Science and Technology (DST), India, Grant No. DST/ICPS/QuST/Theme-1/2019/23. We acknowledge the use of a modern PYTHON library for general-purpose condensed-matter physics [75,76] and the cluster computing facility at Harish-Chandra Research Institute.

APPENDIX A: TWO-SITE TWO-PARTICLE SYSTEM

Let us consider the scenario in which the lattice has two sites occupied by two bosonic particles. The normalized Hamiltonian in the Fock-state basis looks like

$$H_B^b = \frac{1}{\sqrt{16J^{b2}+U^{b2}}}\begin{bmatrix} U^b & -2\sqrt{2}J^b & 0 \\ -2\sqrt{2}J^b & -U^b & -2\sqrt{2}J^b \\ 0 & -2\sqrt{2}J^b & U^b \end{bmatrix}. \tag{A1}$$

The initial state $\rho(0)$ of the system is the ground state of this Hamiltonian H_B^b, given by

$$\rho(0) = \begin{bmatrix} \frac{1}{4}(1-a) & \sqrt{2}b' & \frac{1}{4}(1-a) \\ \sqrt{2}b' & \frac{1}{2}(1+a) & \sqrt{2}b' \\ \frac{1}{4}(1-a) & \sqrt{2}b' & \frac{1}{4}(1-a) \end{bmatrix}, \tag{A2}$$

where $a = \frac{U^b}{\sqrt{16J^{b2}+U^{b2}}}$ and $b' = \frac{J^b}{\sqrt{16J^{b2}+U^{b2}}}$. We construct the charging Hamiltonian by setting $J^b = 0$, which reads

$$H_c^b = \begin{bmatrix} U_c^b & 0 & 0 \\ 0 & 0 & 0 \\ 0 & 0 & U_c^b \end{bmatrix}. \tag{A3}$$

After evolving the state $\rho(0)$ by the unitary operator $\mathcal{U}_c = \exp(-iH_c^b t)$ for a time interval t, the resultant state $\rho(t)$ becomes

$$\begin{bmatrix} \frac{1}{4}(1-a) & \sqrt{2}b'e^{-itU_c^b} & \frac{1}{4}(1-a) \\ \sqrt{2}b'e^{itU_c^b} & \frac{1}{2}(1+a) & \sqrt{2}b'e^{itU_c^b} \\ \frac{1}{4}(1-a) & \sqrt{2}b'e^{-itU_c^b} & \frac{1}{4}(1-a) \end{bmatrix}. \tag{A4}$$

The average work output can then be computed as

$$W^b(t) = \frac{J^{b2}}{J^{b2}+(0.25U^b)^2}\left[1-\cos\left(tU_c^b\right)\right]. \tag{A5}$$

APPENDIX B: THREE-SITE AND THREE-PARTICLE SCENARIO IN THE ABSENCE OF ON-SITE INTERACTION

Let us consider a lattice with three sites; for the FH model, it has $N_\uparrow^f = 2$ and $N_\downarrow^f = 1$. In the absence of U^f, the three-particle Hamiltonian reads

$$H_B^f = \frac{1}{4\sqrt{2}J^f}\begin{bmatrix} 0 & -2J^f & 0 & -2J^f & 0 & 0 & 0 & 0 & 0 \\ -2J^f & 0 & -2J^f & 0 & -2J^f & 0 & 0 & 0 & 0 \\ 0 & -2J^f & 0 & 0 & 0 & -2J^f & 0 & 0 & 0 \\ -2J^f & 0 & 0 & 0 & -2J^f & 0 & -2J^f & 0 & 0 \\ 0 & -2J^f & 0 & -2J^f & 0 & -2J^f & 0 & -2J^f & 0 \\ 0 & 0 & -2J^f & 0 & -2J^f & 0 & 0 & 0 & -2J^f \\ 0 & 0 & 0 & -2J^f & 0 & 0 & 0 & -2J^f & 0 \\ 0 & 0 & 0 & 0 & -2J^f & 0 & -2J^f & 0 & -2J^f \\ 0 & 0 & 0 & 0 & 0 & -2J^f & 0 & -2J^f & 0 \end{bmatrix}. \tag{B1}$$

Following the same construction procedure as for two lattice sites, the charging Hamiltonian takes the form

$$H_c^f = \mathrm{diag}\{U_c^f, U_c^f, 0, U_c^f, 0, U_c^f, 0, U_c^f, U_c^f\},$$

which leads to the average work for a system composed of fermions as

$$W^f(t) = 0.75\left[1-\cos\left(tU_c^f\right)\right]. \tag{B2}$$

On the other hand, for the BH system with $L = 3$ and $N^b = 3$ with a maximum of two particles per site, the Hamiltonian becomes

$$H_B^b = \frac{1}{(3+\sqrt{17})J^b}\begin{bmatrix} 0 & -2J^b & -4J^b & 0 & 0 & 0 & 0 \\ -2J^b & 0 & 0 & -2\sqrt{2}J^b & 0 & 0 & 0 \\ -4J^b & 0 & 0 & -2\sqrt{2}J^b & 0 & 0 & 0 \\ 0 & -2\sqrt{2}J^b & -2\sqrt{2}J^b & 0 & -2\sqrt{2}J^b & -2\sqrt{2}J^b & 0 \\ 0 & 0 & 0 & -2\sqrt{2}J^b & 0 & 0 & -2J^b \\ 0 & 0 & 0 & -2\sqrt{2}J^b & 0 & 0 & -4J^b \\ 0 & 0 & 0 & 0 & -2J^b & -4J^b & 0 \end{bmatrix}. \tag{B3}$$

In this case, the charging Hamiltonian reads

$$H_c^b = \mathrm{diag}\{U_c^b, U_c^b, U_c^b, 0, 0, U_c^b, U_c^b, U_c^b\},$$

and the average work turns out to be

$$W^b(t) = 0.621\left[1 - \cos\left(tU_c^b\right)\right]. \tag{B4}$$

[1] N. Linden, S. Popescu, and P. Skrzypczyk, Phys. Rev. Lett. **105**, 130401 (2010).

[2] V. Giovannetti, S. Lloyd, and L. Maccone, Nat. Photon. **5**, 222 (2011).

[3] N. Gisin, G. Ribordy, W. Tittel, and H. Zbinden, Rev. Mod. Phys. **74**, 145 (2002).

[4] Y.-H. Yang, P.-Y. Li, S.-Z. Ma, X.-C. Qian, K.-Y. Zhang, L.-J. Wang, W.-L. Zhang, F. Zhou, S.-B. Tang, J.-Y. Wang, Y. Yu, Q. Zhang, and J.-W. Pan, Opt. Express **29**, 25859 (2021).

[5] K. Joulain, J. Drevillon, Y. Ezzahri, and J. Ordonez-Miranda, Phys. Rev. Lett. **116**, 200601 (2016).

[6] G. Gemmer, M. Michel, and G. Mahler, *Quantum Thermodynamics* (Springer, New York, 2004).

[7] S. Vinjanampathy and J. Anders, Contemp. Phys. **57**, 545 (2016).

[8] A. Hewgill, J. O. González, J. P. Palao, D. Alonso, A. Ferraro, and G. De Chiara, Phys. Rev. E **101**, 012109 (2020).

[9] M. T. Mitchison, M. P. Woods, J. Prior, and M. Huber, New J. Phys. **17**, 115013 (2015).

[10] L. A. Correa, J. P. Palao, G. Adesso, and D. Alonso, Phys. Rev. E **87**, 042131 (2013).

[11] J. B. Brask and N. Brunner, Phys. Rev. E **92**, 062101 (2015).

[12] S. Das, A. Misra, A. K. Pal, A. Sen(De), and U. Sen, Europhys. Lett. **125**, 20007 (2019).

[13] R. Alicki and M. Fannes, Phys. Rev. E **87**, 042123 (2013).

[14] J. M. Zhang and R. X. Dong, Eur. J. Phys. **31**, 591 (2010).

[15] F. Zhao, F.-Q. Dou, and Q. Zhao, Phys. Rev. A **103**, 033715 (2021).

[16] F. C. Binder, S. Vinjanampathy, K. Modi, and J. Goold, New J. Phys. **17**, 075015 (2015).

[17] F. Campaioli, F. A. Pollock, F. C. Binder, L. Céleri, J. Goold, S. Vinjanampathy, and K. Modi, Phys. Rev. Lett. **118**, 150601 (2017).

[18] S. Ghosh, T. Chanda, and A. Sen(De), Phys. Rev. A **101**, 032115 (2020).

[19] D. Rossini, G. M. Andolina, D. Rosa, M. Carrega, and M. Polini, Phys. Rev. Lett. **125**, 236402 (2020).

[20] A. C. Santos, B. Çakmak, S. Campbell, and N. T. Zinner, Phys. Rev. E **100**, 032107 (2019).

[21] F.-Q. Dou, Y.-J. Wang, and J.-A. Sun, Europhys. Lett. **131**, 43001 (2020).

[22] S. Ghosh, T. Chanda, S. Mal, and A. Sen(De), Phys. Rev. A **104**, 032207 (2021).

[23] F. Campaioli, F. A. Pollock, and S. Vinjanampathy, Quantum batteries, in *Thermodynamics in the Quantum Regime: Fundamental Aspects and New Directions*, edited by F. Binder, L. A. Correa, C. Gogolin, J. Anders, and G. Adesso (Springer International Publishing, Cham, Switzerland, 2018), pp. 207–225.

[24] D. Ferraro, M. Campisi, G. M. Andolina, V. Pellegrini, and M. Polini, Phys. Rev. Lett. **120**, 117702 (2018).

[25] G. M. Andolina, M. Keck, A. Mari, V. Giovannetti, and M. Polini, Phys. Rev. B **99**, 205437 (2019).

[26] K. V. Hovhannisyan, M. Perarnau-Llobet, M. Huber, and A. Acín, Phys. Rev. Lett. **111**, 240401 (2013).

[27] J.-Y. Gyhm, D. Šafránek, and D. Rosa, Phys. Rev. Lett. **128**, 140501 (2022).

[28] F. Barra, Phys. Rev. Lett. **122**, 210601 (2019).

[29] J. Liu, D. Segal, and G. Hanna, J. Phys. Chem. C **123**, 18303 (2019).

[30] D. Farina, G. M. Andolina, A. Mari, M. Polini, and V. Giovannetti, Phys. Rev. B **99**, 035421 (2019).

[31] J. Q. Quach and W. J. Munro, Phys. Rev. Applied **14**, 024092 (2020).

[32] Á. Tejero, J. Thingna, and D. Manzano, J. Phys. Chem. C **125**, 7518 (2021).

[33] T. P. Le, J. Levinsen, K. Modi, M. M. Parish, and F. A. Pollock, Phys. Rev. A **97**, 022106 (2018).

[34] S. Ghosh and A. Sen(De), Phys. Rev. A **105**, 022628 (2022).

[35] J. Q. Quach, K. E. McGhee, L. Ganzer, D. M. Rouse, B. W. Lovett, E. M. Gauger, J. Keeling, G. Cerullo, D. G. Lidzey, and T. Virgili, Sci. Adv. **8**, eabk3160 (2022).

[36] C.-K. Hu, J. Qiu, P. J. P. Souza, J. Yuan, Y. Zhou, L. Zhang, J. Chu, X. Pan, L. Hu, J. Li, Y. Xu, Y. Zhong, S. Liu, F. Yan, D. Tan, R. Bachelard, C. J. Villas-Boas, A. C. Santos, and D. Yu, Quantum Sci. Technol. **7**, 045018 (2022).

[37] M. Lewenstein, A. Sanpera, V. Ahufinger, B. Damski, A. Sen(De), and U. Sen, Adv. Phys. **56**, 243 (2007).

[38] I. Bloch, J. Dalibard, and W. Zwerger, Rev. Mod. Phys. **80**, 885 (2008).

[39] T. Esslinger, Annu. Rev. Condens. Matter Phys. **1**, 129 (2010).

[40] O. Dutta, M. Gajda, P. Hauke, M. Lewenstein, D.-S. Lühmann, B. A. Malomed, T. Sowiński, and J. Zakrzewski, Rep. Prog. Phys. **78**, 066001 (2015).

[41] M. P. A. Fisher, P. B. Weichman, G. Grinstein, and D. S. Fisher, Phys. Rev. B **40**, 546 (1989).

[42] L. D. Carr and M. J. Holland, Phys. Rev. A **72**, 031604(R) (2005).

[43] J. K. Freericks and H. Monien, Europhys. Lett. **26**, 545 (1994).

[44] D. Rossini and R. Fazio, New J. Phys. **14**, 065012 (2012).

[45] C. Fort, L. Fallani, V. Guarrera, J. E. Lye, M. Modugno, D. S. Wiersma, and M. Inguscio, Phys. Rev. Lett. **95**, 170410 (2005).

[46] L. Fallani, J. E. Lye, V. Guarrera, C. Fort, and M. Inguscio, Phys. Rev. Lett. **98**, 130404 (2007).

[47] M. White, M. Pasienski, D. McKay, S. Q. Zhou, D. Ceperley, and B. DeMarco, Phys. Rev. Lett. **102**, 055301 (2009).

[48] B. Shapiro, J. Phys. A **45**, 143001 (2012).

[49] V. Ahufinger, L. Sanchez-Palencia, A. Kantian, A. Sanpera, and M. Lewenstein, Phys. Rev. A **72**, 063616 (2005).

[50] B. Damski, J. Zakrzewski, L. Santos, P. Zoller, and M. Lewenstein, Phys. Rev. Lett. **91**, 080403 (2003).

[51] A. Aharony, Phys. Rev. B **18**, 3328 (1978).

[52] B. J. Minchau and R. A. Pelcovits, Phys. Rev. B **32**, 3081 (1985).

[53] J. Wehr, A. Niederberger, L. Sanchez-Palencia, and M. Lewenstein, Phys. Rev. B **74**, 224448 (2006).

[54] D. A. Abanin, P. A. Lee, and L. S. Levitov, Phys. Rev. Lett. **98**, 156801 (2007).

[55] J. Hide, W. Son, and V. Vedral, Phys. Rev. Lett. **102**, 100503 (2009).

[56] A. Niederberger, M. M. Rams, J. Dziarmaga, F. M. Cucchietti, J. Wehr, and M. Lewenstein, Phys. Rev. A **82**, 013630 (2010).

[57] R. Prabhu, S. Pradhan, A. Sen(De), and U. Sen, Phys. Rev. A **84**, 042334 (2011).

[58] D. Sadhukhan, S. S. Roy, D. Rakshit, R. Prabhu, A. Sen(De), and U. Sen, Phys. Rev. E **93**, 012131 (2016).

[59] P. W. Anderson, Phys. Rev. **109**, 1492 (1958).

[60] D. A. Abanin, E. Altman, I. Bloch, and M. Serbyn, Rev. Mod. Phys. **91**, 021001 (2019).

[61] J. H. Bardarson, F. Pollmann, and J. E. Moore, Phys. Rev. Lett. **109**, 017202 (2012).

[62] A. Pal and D. A. Huse, Phys. Rev. B **82**, 174411 (2010).

[63] E. Canovi, D. Rossini, R. Fazio, G. E. Santoro, and A. Silva, Phys. Rev. B **83**, 094431 (2011).

[64] B. Rosenstein and D. Li, Rev. Mod. Phys. **82**, 109 (2010).

[65] M. Moeckel and S. Kehrein, Phys. Rev. Lett. **100**, 175702 (2008).

[66] D. Chen, M. White, C. Borries, and B. DeMarco, Phys. Rev. Lett. **106**, 235304 (2011).

[67] B. Bertini, E. Tartaglia, and P. Calabrese, J. Stat. Mech. (2017) 103107.

[68] F. Hulpke, U. V. Poulsen, A. Sanpera, A. Sen(De), U. Sen, and M. Lewenstein, Found. Phys. **36**, 477 (2006).

[69] M. N. Bera, A. Riera, M. Lewenstein, Z. B. Khanian, and A. Winter, Quantum **3**, 121 (2019).

[70] H. Gimperlein, S. Wessel, J. Schmiedmayer, and L. Santos, Phys. Rev. Lett. **95**, 170401 (2005).

[71] P. Sierant, D. Delande, and J. Zakrzewski, Phys. Rev. A **95**, 021601(R) (2017).

[72] A. Kauch, P. Worm, P. Prauhart, M. Innerberger, C. Watzenböck, and K. Held, Phys. Rev. B **102**, 245125 (2020).

[73] A quenched averaged quantity of any physical observable M calculated over a random distribution $\{Y_j\}$ with a given mean $\langle Y\rangle$ and standard deviation σ_Y is calculated as $\langle M(\langle Y\rangle, \sigma_Y)\rangle = \int\int\cdots\int M\{Y_j\}d\{Y_j\}$.

[74] P. J. H. Denteneer, R. T. Scalettar, and N. Trivedi, Phys. Rev. Lett. **83**, 4610 (1999).

[75] P. Weinberg and M. Bukov, SciPost Phys. **2**, 003 (2017).

[76] P. Weinberg and M. Bukov, SciPost Phys. **7**, 020 (2019).